IOP Conference Series: Earth and Environmental Science

PAPER • **OPEN ACCESS**

Modeling And Simulation Of Doubly-Fed Induction Generator Based On ADPSS

To cite this article: Shengnan Li *et al* 2018 *IOP Conf. Ser.: Earth Environ. Sci.* **186** 012003

View the article online for updates and enhancements.

You may also like

- Current source converter-based optimal power extraction and power control of a doubly fed induction generator (DFIG) using backstepping control
Ram Krishan Kumar and Jayanti Choudhary
- Analysis of Vector Controlled Variable Speed DFIG for Wind Turbines
Talib Z. Farge, Ali H. Numan and Ghasaq M. Hussein
- All-fiber cylindrical vector beams laser based on an acoustically-induced fiber grating
Xuecheng Zhang, Wending Zhang, Chenyang Li et al.

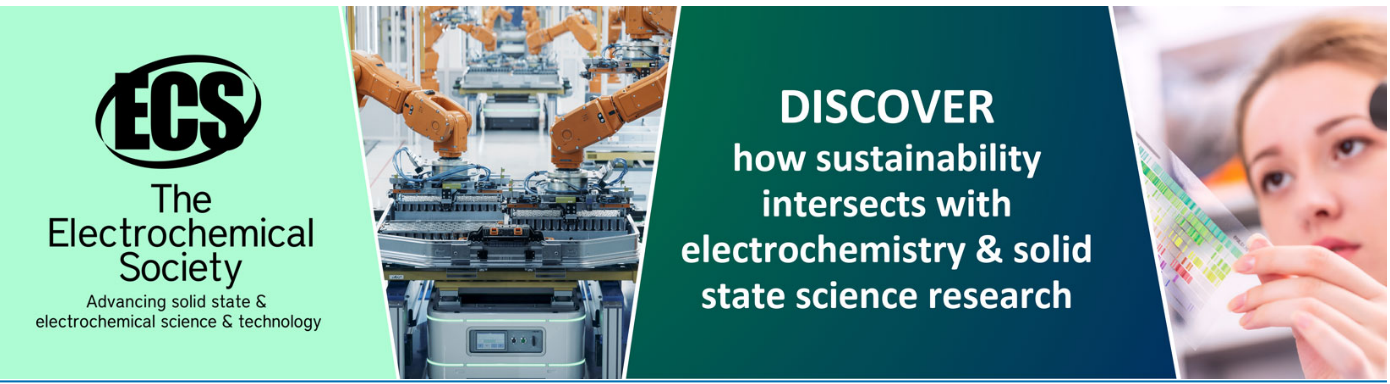

This content was downloaded from IP address 3.147.73.147 on 21/05/2024 at 08:17

IOP Conf. Series: Earth and Environmental Science **186** (2018) 012003 doi:10.1088/1755-1315/186/5/012003

Modeling And Simulation Of Doubly-Fed Induction Generator Based On ADPSS

Shengnan Li [1], Peng He [1], Xiaoyu Guo [1], Tingyi He [1]

[1]The Electric Power Research Institute of Yunnan Electric Power Grid,

NO. 105 YUNDAXI ROAD GUANDU DISTRICT 650217, KUNMING YUNNAN CHINA

Abstract. In this paper, the aerodynamic model, machine model, converter model and control model of Doubly-Fed Induction Generator (DFIG) are introduced. The simulation model of DFIG system is established in ADPSS by a self-defined mathematics module. The simulation results show that the control target is achieved and the best speed of rotor can still be maintained under the change of wind speed. The constructed simulation model can accurately reflect the electromagnetic dynamic characteristics of the DIFG wind power generation system and provide an effective simulation platform for the control system design and analysis of the DIFG.

1. Introduction

As a clean and renewable energy source, wind energy has great potential for development. Therefore, wind energy is increasingly valued by countries around the world. At present, many major developed and developing countries in the world have already made great efforts to develop renewable energy such as wind power as an important means to cope with the increasingly severe energy crisis and challenges of climate change. With the rapid development of wind power technology and equipment in the world, wind power has become the renewable energy technology with the most mature technology, the most extensive development conditions and commercial development prospects. Under the guidance of the national renewable energy strategy, China's wind power has achieved rapid development. By 2017, the cumulative grid capacity of wind power in China will be 160 million kilowatts. Compared with the fixed-speed wind generator, the speed of DFIG is adjustable, which can improve the efficiency of wind energy absorption and realize the decoupling control of active and reactive power [1-2]. However, the structure of DFIG is more complex. As an important research method, the modelling of DFIG is particularly important [3-6]. In this paper, based on the mathematical model of the DFIG, the DFIG model is established by the self-defined mathematical function in ADPSS and the effectiveness of the DFIG control system is verified by simulation.

2. Model and control strategy of DFIG

The model of DFIG system includes an aerodynamic model, a machine model, a converter model, a control model, etc. FIG. 1 is a schematic diagram of a DFIG system.

Content from this work may be used under the terms of the Creative Commons Attribution 3.0 licence. Any further distribution of this work must maintain attribution to the author(s) and the title of the work, journal citation and DOI.
Published under licence by IOP Publishing Ltd

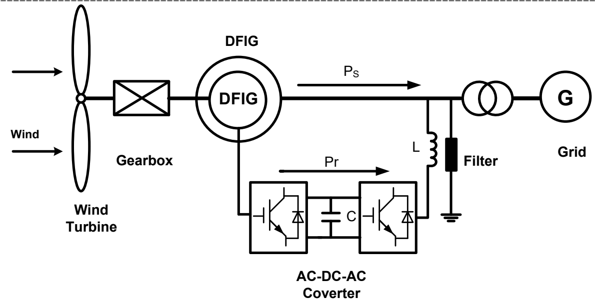

Fig. 1 A DFIG system schematic

2.1. Aerodynamic model

From aerodynamics, the mechanical power generated by the wind turbine [7-8] is:

$$\begin{cases} P_m = \dfrac{1}{2}\rho\pi R^2 v^3 C_p(\lambda,\beta) \\ \lambda = \dfrac{R\omega_r}{v} \end{cases} \tag{1}$$

Where: ρ is the density of air. R is the radius of turbine. ωr is the speed of rotor. v is the speed of wind. λ is tip-speed ratio. β is the pitch angle. Cp is capacity utilization factor. Pm is the mechanical power of shaft.

2.2. Model of the doubly fed induction machine

The electromagnetic transient voltage model of the doubly-fed induction machine in the dq coordinate system can be written by the voltage and flux equation of the dq axis using Parker transform:

$$\begin{bmatrix} u_{ds} \\ u_{qs} \\ u_{dr} \\ u_{qr} \end{bmatrix} = \begin{bmatrix} \rho L_s + r_s & -\omega_0 L_s & \rho L_m & -\omega_0 L_m \\ \omega_0 L_s & \rho L_s + r_s & \omega_0 L_m & \rho L_m \\ \rho L_m & -s\omega_0 L_m & \rho L_r + r_r & -s\omega_0 L_r \\ s\omega_0 L_m & \rho L_m & s\omega_0 L_r & \rho L_r + r_r \end{bmatrix} \begin{bmatrix} i_{ds} \\ i_{qs} \\ i_{dr} \\ i_{qr} \end{bmatrix} \tag{2}$$

The active power and reactive power absorbed by the stator are:

$$\begin{cases} P_s = \dfrac{3}{2}(u_{ds}i_{ds} + u_{qs}i_{qs}) \\ Q_s = \dfrac{3}{2}(u_{qs}i_{ds} - u_{ds}i_{qs}) \end{cases} \tag{3}$$

2.3. Converter control model

With stator flux orientation, the stator flux vector lags behind the stator terminal voltage vector by 90 degrees, from which the flux observer can be constructed. The active power and reactive power absorbed by the stator side are respectively controlled by the torque component i_{qr} and the excitation component i_{dr} of the rotor current. By controlling i_{qr} and i_{dr}, the active and reactive power of the machine can be instantaneously controlled. In practice, the following approximate formula is often used because the flux cannot be measured accurately:

$$\begin{cases} P_s = -\frac{3}{2}U_s \frac{L_m}{L_s} i_{qr} \\ Q_s = \frac{3}{2}U_s (\frac{U_s}{L_s \omega_0} - \frac{L_m}{L_s} i_{dr}) \end{cases} \tag{4}$$

The entire system is a double closed-loop control structure. The outer ring is a power control loop and the inner loop is a current control loop. The stator active power Ps and the stator reactive power Qs are calculated from the detected stator and rotor voltages and currents and they are compared with the given values P*s and Q* of the stator active and reactive power. The given value of rotor current i*qr and i*dr is generated after PI regulation. The given values i*qr and i*dr are compared with the actual feedback iqr and idr and fed to the PI regulator to obtain the control voltages on the d and q axes. After reversed Park transformation, the control voltage component in the three-phase coordinate system can be obtained.

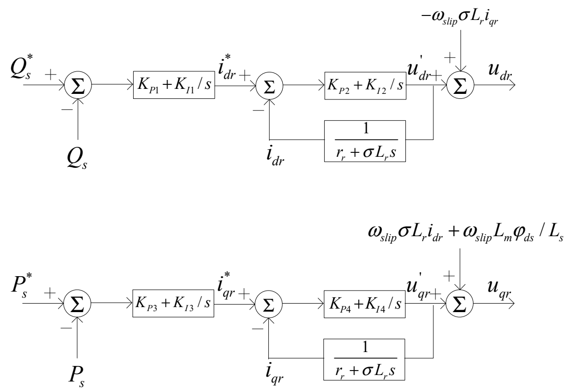

Fig. 2 Control loops of active power and reactive power on rotor side

For the grid-side converter, it is specified that the current flowing into the converter is positive, and the following circuit equation holds:

$$\begin{cases} u_{ag} = L_g p i_{ag} + r_g i_{ag} + u_{agc} \\ u_{bg} = L_g p i_{bg} + r_g i_{bg} + u_{bgc} \\ u_{cg} = L_g p i_{cg} + r_g i_{cg} + u_{cgc} \end{cases} \tag{5}$$

After the Parker transformation, the dq axis equation can be obtained:

$$\begin{cases} u_{dg} = L_g p i_{dg} + r_g i_{dg} - \omega_0 L_g i_{qg} + u_{dgc} \\ u_{qg} = L_g p i_{qg} + r_g i_{qg} + \omega_0 L_g i_{dg} + u_{qgc} \end{cases} \tag{6}$$

By using voltage-oriented control $u_{dg} = U_s$, $u_{qg} = 0$, the power equation is:

$$\begin{cases} P_g = \frac{3}{2}U_s i_{dg} \\ Q_g = -\frac{3}{2}U_s i_{qg} \end{cases} \tag{7}$$

The active power Pg and reactive power Qg exchanged between the grid-side converter and the grid are controlled by idg and iqg, respectively, and the DC voltage can be controlled by the active current idg [9-10]. The reactive current iqg controls the AC side voltage and the phase of current(ie reactive power). Therefore, for the grid-side converter, the control target of the active power is to keep the DC voltage constant; the control target of the reactive power is to send the specified value of reactive power.

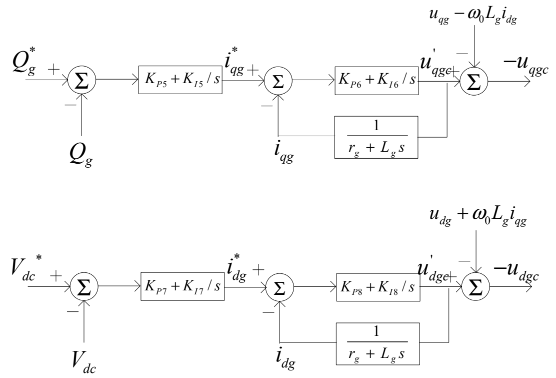

Fig. 3 Grid-side active power control loop and reactive power control loop

3. Design of double closed-loop control system

The entire system is a double closed-loop control structure. The outer loop is a power control loop and the inner loop is a current control loop. Rewrite the simplified rotor circuit equation into the standard structure of the dynamic equation:

$$\begin{cases}\left(L_r-\dfrac{L_m^2}{L_s}\right)pi_{dr}=-r_r i_{dr}+u_{dr}+s\omega_0\left(L_r-\dfrac{L_m^2}{L_s}\right)i_{qr}\\\left(L_r-\dfrac{L_m^2}{L_s}\right)pi_{qr}=-r_r i_{qr}+u_{qr}-s\omega_0\left(L_r-\dfrac{L_m^2}{L_s}\right)i_{dr}-s\omega_0\dfrac{L_m}{L_s}\varphi_{ds}\end{cases}\tag{8}$$

It can be seen from the above equation that the d and q axis components of the rotor current can be controlled by the d and q axis components of the rotor voltage respectively. But the effects of the coupling and the stator flux interfere with the rotor voltage control of the rotor current. It can be treated as a disturbance of the system.

Closed-loop has the ability to eliminate the disturbance in the ring, but the disturbance will reduce the dynamic and static characteristics of the current closed-loop system. In this case, the disturbance needs to be compensated. Δu_{dr} and Δu_{qr} are the rotor side compensation voltages of d and q axis, as shown below:

$$\begin{cases}\Delta u_{dr}=s\omega_0\left(L_r-\dfrac{L_m^2}{L_s}\right)i_{qr}\\\Delta u_{qr}=-s\omega_0\left(L_r-\dfrac{L_m^2}{L_s}\right)i_{dr}-s\omega_0\dfrac{L_m}{L_s}\varphi_{ds}\end{cases}\tag{9}$$

Let $u'_{dr}=u_{dr}+\Delta u_{dr}$, $u'_{qr}=u_{qr}+\Delta u_{qr}$, Leakage coefficient $\sigma=1-\dfrac{L_m^2}{L_s L_r}$. Then the rotor circuit equation can be written as:

$$\begin{cases}\sigma L_r pi_{dr}=-r_r i_{dr}+u'_{dr}\\\sigma L_r pi_{qr}=-r_r i_{qr}+u'_{qr}\end{cases}\tag{10}$$

The corresponding transfer function is:

$$\frac{i_{dr}}{u_{dr}^{'}} = \frac{i_{qr}}{u_{qr}^{'}} = \frac{1}{r_r + \sigma L_r p} \tag{11}$$

3.1 Inner ring PI parameters of active power loop

For the current inner loop: The closed loop transfer function of the current and current reference values is:

$$\frac{i_{qr}}{i_{qr}^*} = \frac{(K_{P4} + \frac{K_{I4}}{p}) * \frac{1}{(r_r + \sigma L_r p)}}{1 + (K_{P4} + \frac{K_{I4}}{p}) * \frac{1}{(r_r + \sigma L_r p)}} \tag{12}$$

To obtain a Type 1 closed-loop transfer function and to eliminate the steady-state error under the unit step response, equation (13) must hold:

$$\frac{i_{qr}}{i_{qr}^*} = \frac{\alpha_4}{p + \alpha_4} = \frac{\frac{\alpha_4}{p}}{1 + \frac{\alpha_4}{p}} \tag{13}$$

Compare the two equations above:

$$(K_{P4} + \frac{K_{I4}}{p}) * \frac{1}{(r_r + \sigma L_r p)} = \frac{\alpha_4}{p} \tag{14}$$

Thus the PI parameters are:

$$\begin{cases} K_{P4} = \alpha_4 \sigma L_r \\ K_{I4} = \alpha_4 r_r \end{cases} \tag{15}$$

3.2 Outer ring PI parameters of active power loop

The designed inner current loop system is regarded as part of the outer power loop and the closed loop transfer function of the outer power loop power and power reference value is:

$$\frac{P_s}{P_s^*} = \frac{(K_{P3} + \frac{K_{I3}}{p}) * \frac{\alpha_4}{p + \alpha_4} * (-\frac{3}{2} U_s \frac{L_m}{L_s})}{1 + (K_{P3} + \frac{K_{I3}}{p}) * \frac{\alpha_4}{p + \alpha_4} * (-\frac{3}{2} U_s \frac{L_m}{L_s})} \tag{16}$$

To get $\frac{P_s}{P_s^*} = \frac{\alpha_3}{p + \alpha_3}$, we have:

$$\begin{cases} K_{P3} = \alpha_3 / \alpha_4 / (-\frac{3}{2} U_s \frac{L_m}{L_s}) \\ K_{I3} = \alpha_3 / (-\frac{3}{2} U_s \frac{L_m}{L_s}) \end{cases} \tag{17}$$

3.3 Inner current ring and outer power ring PI parameters of reactive power loop

The inner current loop of the reactive loop is the same as the inner current loop of the active loop, so there is:

$$\begin{cases} K_{P2} = \alpha_2 \sigma L_r \\ K_{I2} = \alpha_2 r_r \end{cases} \tag{18}$$

Use the same method as the active loop, we get:

$$\begin{cases} K_{P1} = \alpha_1 / \alpha_2 / (-\frac{3}{2} U_s \frac{L_m}{L_s}) \\ K_{I1} = \alpha_1 / (-\frac{3}{2} U_s \frac{L_m}{L_s}) \end{cases} \tag{19}$$

4. Simulation verification

4.1. Simulation system

Simulation systems mainly include DFIG, converters, and wind turbines (implemented in the UD). The DFIG system is connected to the infinite bus.

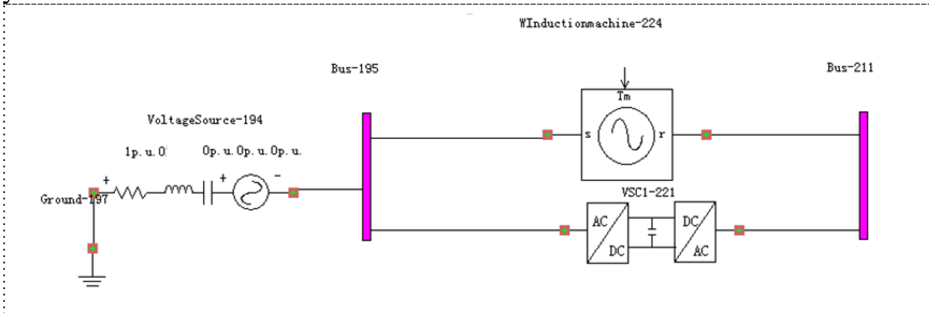

Figure 4 Simulation System

DFIG parameters : radius of turbine R=4.3m, rated power Pn=15kW, DC side rated voltage V dc=1000, Rated line to neutral voltage U N=380V, DC capacitor C=2000uF, line reactor Lg=0.005H, rated frequency f=50Hz, number of pole pairs p = 3, moment of inertia J g=0.39kgm2, stator resistance R1=0.0379Ω, Stator leakage inductance L1=0.0011H, rotor resistance R2=0.031Ω, rotor leakage inductance L2=0.0022H, mutual inductance Lm=0.0427H.

4.2 Control parameter calculation

The outer loop system has no steady state errors and the rise time is no more than 0.02 s. For a first-order transfer function of the form $G_s = \frac{1}{Ts+1}$, the formula for obtaining the rise time of the step response according to the first-order system $t_r = 2.20T$. For inner loop control parameters, there is $0.002 = 2.20 * T * (1+20\%)$, which is $T = 7.5758\text{e-}004$, corresponding closed-loop poles a = 1320. For outer loop control parameter $T = 7.5758\text{e-}003$, corresponding closed-loop poles a = 132.

Table 1. PI Parameters of Current Loop and Power Loop

Circuit	Inner current loop KP parameters	Inner current loop KI parameters	Outer power loop KP parameters	Outer power loop KI parameters
Rotor-side converter active power	4.3206	41.448	-0.0002204	-0.2909
Rotor-side converter reactive power	4.3206	41.448	-0.0002204	-0.2909
Grid-side converter active power	6.6	0	0.0002836	0.03744

Grid-side converter reactive power	*6.6*	0	-0.0002148	-0.2836

4.3. Time domain simulation

4.3.1. Simulation Experiment 1: Step Response

The following 4 step response simulation are performed:

1. Step response test of the DC side voltage: the reference value of the DC side voltage is stepped from 1000V to 1050V at 5s.
2. Reactive power step response test of the grid-side converter: the reference value of reactive power is stepped from 0Var to 1000Var at 5s.
3. Reactive power step response test on the stator side of the motor: the reference value of reactive power is stepped from 0Var to 1000Var at 5s.
4. The active power step response test on the stator side of the motor: the reference value of active power is stepped from -4500Var to -4800Var at 5s.

From the simulation test of the four control loops, it can be seen that the step response of the reference value meets the requirements of the controller design, and the closed-loop response performance of the controller is good.

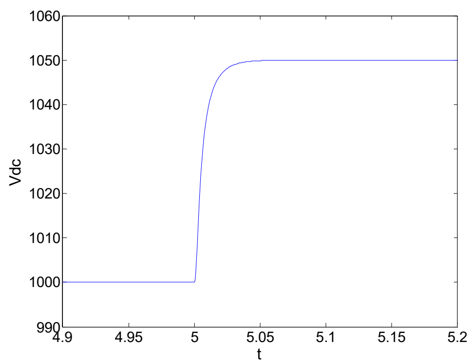

Fig. 5 DC voltage step response curve

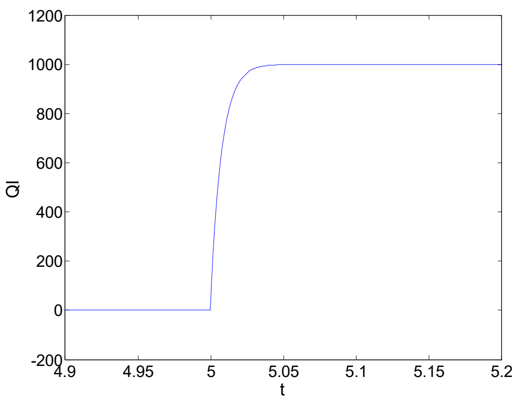

Fig. 6 Reactive power step response curve at the grid side

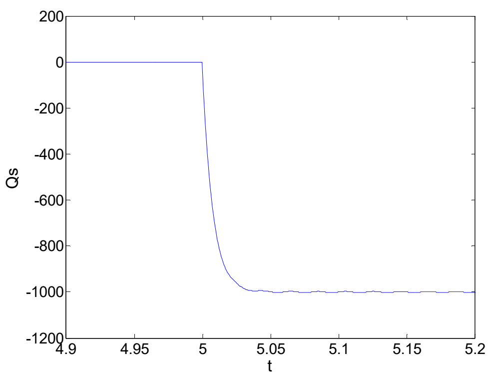

Fig. 7 Stator side reactive power step response curve

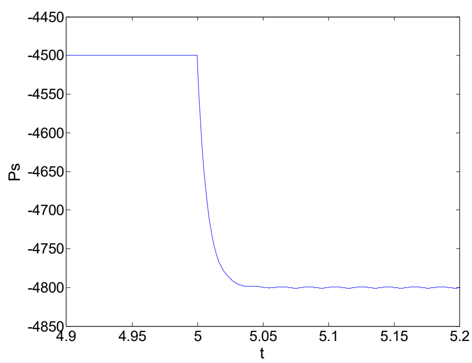

Fig. 8 Active power step response curve on the stator side

IOP Conf. Series: Earth and Environmental Science **186** (2018) 012003 doi:10.1088/1755-1315/186/5/012003

4.3.2. Simulation Experiment 2: Maximum Wind Energy Tracking

The maximum tracking simulation of wind energy [8-9] was verified. The step change of the wind speed was set. The wind speed was stepped from 6.5 m/s to 8.5 m/s at 5 s. Stator current curve of phase a, rotor current curve of phase a, slip rate curve, stator power tracking reference value change curve, utilization coefficient Cp curve and output power of the DFIG were obtained through simulation.

At the moment of wind speed change, the speed of rotor cannot suddenly change and lead to a decrease in Cp. It can be seen that the Psref will decrease first from the maximum wind energy tracking formula. At this point, the utilization factor is reduced but the mechanical torque is greater than the electromagnetic torque and the unit is accelerated due to the increase of wind speed. After about 1 s a new steady state is reached and Cp is still the maximum value. At this time, the corresponding unit slip ratio is s=-0.177230, which is very close to the theoretical value s=-0.1780. It can be seen from the results that the control strategy used achieves the goal of maximum wind energy tracking and can ensure stable economic operation.

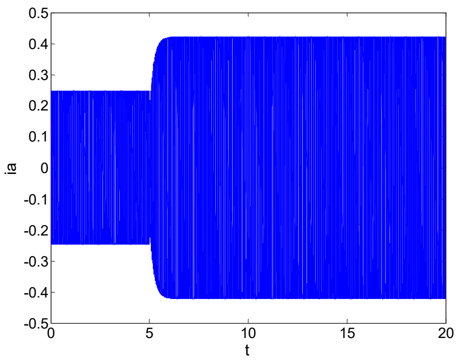

Fig. 9 DFIG stator current of phase a

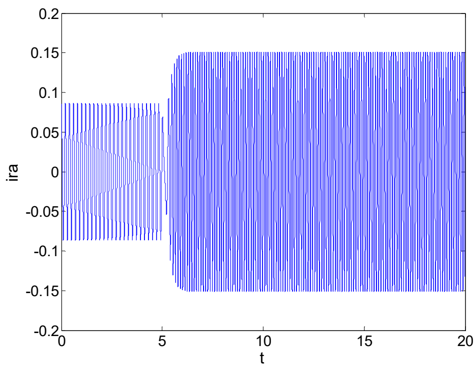

Fig. 10 DFIG rotor current of phase a

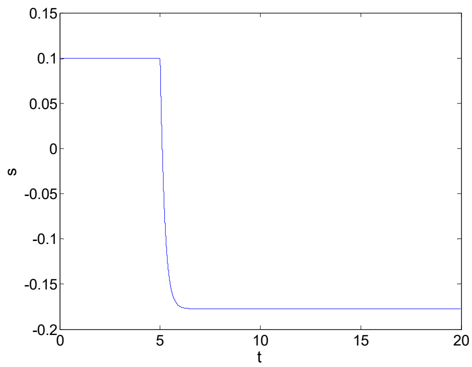

Fig. 11 Slip curve of DFIG

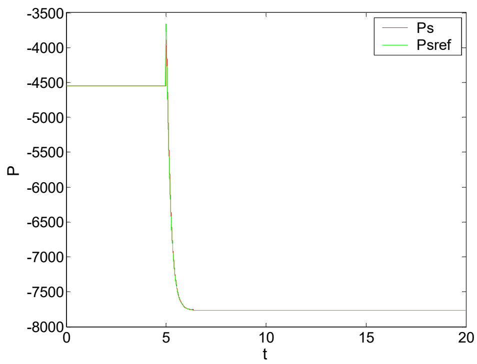

Fig.12 Curve of stator reference power tracking

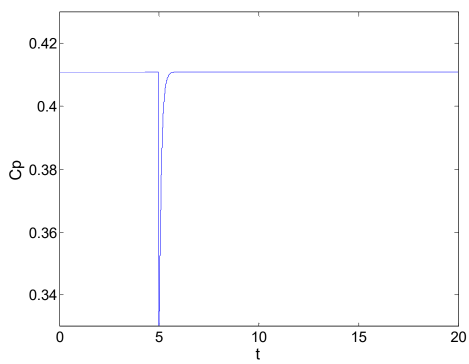

Fig. 13 Curve of utilization coefficient Cp

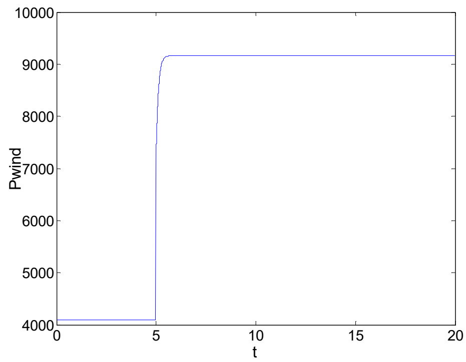

Fig. 14 Output power of DFIG

5. CONCLUSION

The above-mentioned DFIG model and control strategy are verified in ADPSS. The result shows that the control target is achieved and the rotor can still be at the optimum rotation speed under the change of wind speed. The model can accurately reflect the electromagnetic dynamic characteristics of the DFIG system and provide an effective simulation platform for the control design and analysis and calculation of DFIG.

REFERENCES

[1] Slootweg J G, Kling W L, Polinder H. Dynamic modelling of a wind turbine with doubly fed induction generator [C] Power Engineering Society Summer Meeting. [S.l.] : IEEE, 2001:644-649.
[2] Pena R, Clare J C, Asher G M. Doubly fed induction Generator using back-to-back PWM converters and its applicationto variable-speed wind-energy generation [J] . Electric PowerApplications, 1996, 143(3) : 231 - 241.
[3] Koj Abadi H M, Chang L, Boutot T. Novel wind turbine simulator for wind energy conversion systems using an inverter -controlled induction motor [J].IEEE Transactions on Energy Conversion, 2004, 19(3) : 547 - 552.
[4] Mishra Y，Mishra S，Tripathy M，et al. Improving Stability of a DFIG-Based Wind Power System With TunedDamping Controller [J]. IEEE TRANSACTIONS ON ENERGYCONVERSION，2009，24(3):650-660 .
[5] Akhmatovv. Variable speed wind turbines with doubly-fed induction generators. Part I:Modeling in dynamic simulation tools[J].Wind Engineering，2002，26(2):85-108 .
[6] Lucian Mihet-Popa，Frede Blaabjerg，Ion Bolde.Wind TurbineGenerator Modeling and Simulation Where Rotational Speed is the Controlled Variable[J].IEEE TRANSACTIONS ON INDUSTRY APPLICATIONS，2004，40(1):3-10 .
[7] XIANG Da-wei，LI Ran.Control of a doubly fed induction generator in a wind turbine during grid fault ride-through [J].IEEETransaction on Energy Conversion，2006，21(3):652-662 .
[8] LIU Qi - hui, HE Yi - kang, ZHAO Ren - de. The maximal wind-energy tracking control of a variable -speed constant-frequency wind-power generation system[J] . Automation of Electric Power Systems, 2003, 27(20) : 62-67.
[9] JIA Yao - qin, CAO Bing - gang, YANG Zhong - qing. A fastresponse MPPT control method for wind generation [J] . ActaEnergiae Solaris Sinica, 2004, 25(2) : 171-176.